

CELL BIOLOGY

Hindered cytoplasmic diffusion of inositol trisphosphate restricts its cellular range of action

George D. Dickinson,^{1*} Kyle L. Ellefsen,¹ Silvina Ponce Dawson,² John E. Pearson,³ Ian Parker^{1,4}

2016 © The Authors,
some rights reserved;
exclusive licensee
American Association
for the Advancement
of Science.

The range of action of intracellular messengers is determined by their rates of diffusion and degradation. Previous measurements in oocyte cytoplasmic extracts indicated that the Ca^{2+} -liberating second messenger inositol trisphosphate (IP_3) diffuses with a coefficient ($\sim 280 \mu\text{m}^2 \text{s}^{-1}$) similar to that in water, corresponding to a range of action of $\sim 25 \mu\text{m}$. Consequently, IP_3 is generally considered a “global” cellular messenger. We reexamined this issue by measuring local IP_3 -evoked Ca^{2+} puffs to monitor IP_3 diffusing from spot photorelease in neuroblastoma cells. Fitting these data by numerical simulations yielded a diffusion coefficient ($\leq 10 \mu\text{m}^2 \text{s}^{-1}$) about 30-fold slower than that previously reported. We propose that diffusion of IP_3 in mammalian cells is hindered by binding to immobile, functionally inactive receptors that were diluted in oocyte extracts. The predicted range of action of IP_3 ($< 5 \mu\text{m}$) is thus smaller than the size of typical mammalian cells, indicating that IP_3 should better be considered as a local rather than a global cellular messenger.

INTRODUCTION

In a classic paper, Allbritton *et al.* (1) introduced the concept of the “range of action” of an intracellular messenger, specifically considering the distance from a source over which Ca^{2+} ions and inositol trisphosphate (IP_3) can exert their actions. The range of action is determined by how far a messenger can diffuse, on average, before it is removed from the cytosol by degradation (IP_3) or sequestration (Ca^{2+}). To experimentally determine the diffusion rates, Allbritton *et al.* (1) prepared slabs of cytosolic extract from *Xenopus* oocytes and measured the penetration over time of radiolabeled Ca^{2+} and IP_3 presented to one side of a slab after inhibiting degradation and sequestration mechanisms. The apparent diffusion coefficient that they obtained for IP_3 ($283 \pm 53 \mu\text{m}^2 \text{s}^{-1}$) was similar to that expected for free diffusion in a medium with twice the viscosity of water, whereas the value for Ca^{2+} was much lower ($38 \pm 11 \mu\text{m}^2 \text{s}^{-1}$), concordant with hindered diffusion in the presence of immobile Ca^{2+} -binding buffers. Taking into account the respective rates of degradation and sequestration of IP_3 and Ca^{2+} , Sims and Allbritton (2) concluded that Ca^{2+} has a narrow cytosolic range of action and serves as a local signal, whereas IP_3 functions as a global signal because its range of action is greater than the dimensions of typical mammalian cells.

Here, we reconsider the issue of diffusion of IP_3 in the cytosol in light of observations suggesting that binding to immobile sites may appreciably slow the effective diffusion of IP_3 in mammalian cells. In SH-SY5Y neuroblastoma cells and other cell lines, IP_3 primarily evokes Ca^{2+} release from only a few hundred functional IP_3 receptors (IP_3Rs), clustered at discrete sites (3, 4). Different from this, immunostaining of IP_3Rs reveals a dense distribution throughout the cell, and radioligand assays indicate the presence of about 30,000 IP_3R monomers (IP_3 binding sites) per cell (5–8). If these functionally “silent” IP_3Rs bind IP_3 , they would hinder its diffusion without contributing to the Ca^{2+} signal.

We thus set out to determine the effective diffusion coefficient of IP_3 in intact mammalian cells. We uniformly loaded SH-SY5Y cells with a caged, poorly metabolized IP_3 analog (i- IP_3) and selectively photoreleased i- IP_3 using flash photolysis by an ultraviolet (UV) laser spot positioned at one end of these elongated cells. This increased the cytosolic concen-

tration of i- IP_3 at the location of the laser spot, which subsequently equilibrated throughout the cell as free i- IP_3 diffused from the site of origin. To monitor the spread of i- IP_3 , we used IP_3 -evoked Ca^{2+} liberation (Ca^{2+} puffs) from local clusters of IP_3Rs (4, 9) as endogenous and sensitive detectors that are distributed throughout the cell. As previously reported (10), control experiments in which i- IP_3 was uniformly photoreleased across a cell showed that the mean latency between photorelease and the occurrence of the first puff at a site shortened in about linear proportion with increasing concentration of i- IP_3 , whereas the latency did not vary systematically along the length of the cell. Thus, we could use the mean puff latency at sites at different distances from the laser spot as a measure of the temporal profile of the concentration of i- IP_3 ([i- IP_3]) at those locations. If i- IP_3 were to diffuse sufficiently rapidly that its concentration neared equilibrium within the mean first-puff latency, then we would expect similar latencies at all locations. Instead, we observed that the mean first-puff latencies were about 20 times longer at the distal end of the cells as compared to the sites proximate to the UV spot. By comparing these data to model predictions, we derive an estimate for the effective diffusion coefficient of IP_3 in the cytosol of 5 to $10 \mu\text{m}^2 \text{s}^{-1}$, about 30-fold lower than the widely accepted value obtained by Allbritton *et al.* (1). We therefore propose that IP_3 is better considered as a local, rather than a global, messenger in mammalian cells.

RESULTS

Puffs evoked by localized and distributed photorelease of i- IP_3

We loaded SH-SY5Y cells with the Ca^{2+} indicator Fluo-4 and a caged precursor of i- IP_3 , an analog of IP_3 that is slowly metabolized (11) and evokes Ca^{2+} puffs that persist in the cells after flash photorelease with little diminution in mean frequency for more than 2 min (3, 4, 12). During the time course of recordings (30 s), we assumed that degradation of i- IP_3 was negligible so that the total amount that was photoreleased could be assumed to remain constant. Moreover, the latencies of puffs evoked by a given, spatially uniform photolysis flash showed only a small variation between different cells (SD, 40% of mean; 24 cells), indicating a relatively consistent loading of caged i- IP_3 . We also loaded the cells with the slow Ca^{2+} buffer EGTA to suppress global Ca^{2+} waves that could be triggered by the released Ca^{2+} (13). Localized transient Ca^{2+} puffs were evoked by photoreleasing i- IP_3 using a focused laser spot of 405-nm light that was either stationary and positioned so that it illuminated

¹Department of Neurobiology and Behavior, University of California, Irvine, CA 92697, USA. ²Departamento de Física, FCEN-UBA and IFIBA, CONICET, Buenos Aires, Argentina. ³Theoretical Biology and Biophysics, T-10 MS K710, Los Alamos National Laboratory, Los Alamos, NM 87545, USA. ⁴Department of Physiology and Biophysics, University of California, Irvine, CA 92697, USA.

*Corresponding author. Email: dickingsg@uci.edu

within one end of a cell (spot flash) or was rapidly and uniformly stepped across the length of the cell (distributed flash) (Fig. 1A). In both cases, the intensity and total duration of the laser flash were identical, delivering the same number of photons and, hence, photoreleasing the same average amount of $i\text{-IP}_3$. However, because of the difference in spatial profile of the photoreleased $i\text{-IP}_3$, we expected that the spot flash stimulation would evoke puffs beginning, on average, after longer latencies at greater distances from the spot because of the time scale and dilution imposed if $i\text{-IP}_3$ were to diffuse slowly, whereas the distributed flash stimulation would result in a rapid and near-homogeneous increase in $[i\text{-IP}_3]$ throughout the cell.

We mapped the locations of puffs evoked by photoreleased IP_3 throughout a 30-s recording (Fig. 1B) and monitored the fluorescence

ratio traces ($\Delta F/F_0$) from regions of interest centered on these sites (Fig. 1C). We measured the latency to the first puff at each site as a function of the distance of the site from the spot flash (Fig. 1D, top panel) or to the lower end of cells receiving distributed flash stimulation (Fig. 1D, bottom panel). Although there was considerable scatter in the data, these plots showed that puff latencies were longer at sites more distant from the stationary laser spot, whereas there was no obvious systematic variation of puff latency with the positions along the cell in the case of the distributed stimulation.

Determination of mean first-puff latencies

Puffs are stochastic events, and their latencies after spatially uniform photorelease of a given amount of IP_3 are exponentially distributed (9, 10). To obtain estimates of mean latencies by pooling data from multiple puff sites in many cells, we automated the detection and localization of puffs using a freely available custom software algorithm (14). This algorithm reported the latency of each event from the beginning of the photolysis flash together with the distance from the centroid locations of a puff in relation to the spot flash or, arbitrarily, to one end of the cell in trials with distributed flash stimulation. Trials with spot flash and distributed flash stimulation were performed in alternating order, using a constant intensity and differing total flash durations (100, 200, and 500 ms).

Individual first-puff latencies evoked by spot flash of $i\text{-IP}_3$ with flash durations of 100, 200, or 500 ms showed considerable variability (Fig. 2A), as expected, but mean latencies calculated by binning the data points over $\sim 5\text{-}\mu\text{m}$ increments revealed a dependence on distance from the site of photorelease for all three flash durations (Fig. 2B). Mean puff latencies at sites near the laser spot were shorter for longer flash durations but lengthened to ~ 10 s for all flash durations at the end of the cell farthest from the spot flash stimulation site. In contrast, distributed flash stimulation of $i\text{-IP}_3$ throughout the cell evoked puffs with latencies that lacked a systematic relationship with the location along the cell but, on average, shortened progressively with increasing flash duration (Fig. 2, C and D). To further validate the difference in spatial distribution of first-puff latencies between the spot flash and distributed photorelease of $i\text{-IP}_3$, we performed a linear regression to fit a linear function of the distance along the cell to the logarithm of the individual first-puff latencies, as plotted in Fig. 2 (A and C). Latencies depended strongly on the distance from the spot flash stimulation for all flash durations, as manifested by slopes differing significantly

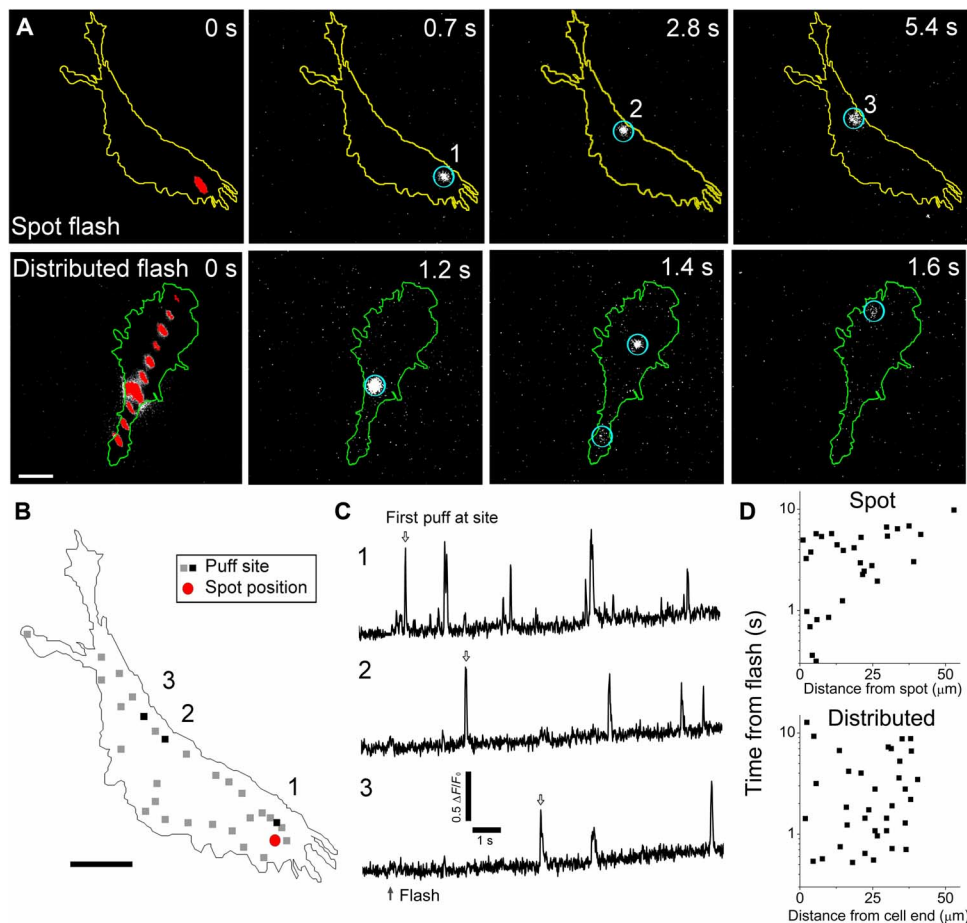


Fig. 1. Latencies of Ca^{2+} puffs evoked by localized and distributed laser spot photorelease of $i\text{-IP}_3$. (A) The top row of panels shows the location of a stationary laser spot flash (200-ms duration) delivered to an SH-SY5Y cell at time 0 (red spot, left panel), and image frames at different times after the flash showing the first puffs arising at select locations (circled). Fluorescence of Fluo-4 during puffs is depicted on an arbitrary gray scale. The bottom row of panels shows corresponding images in a different cell, where a laser flash of the same intensity and total duration was distributed as 10 individual spots spaced evenly along the length of the cell. Scale bar, $10\ \mu\text{m}$. (B) Map of the same cell as in the top row of (A), showing the locations of the puffs numbered in (A) as black squares, the locations of all other identified puff sites marked as gray squares, and the location of the stationary laser spot marked by the red circle. Scale bar, $10\ \mu\text{m}$. (C) Representative traces showing Ca^{2+} -dependent fluorescence ratio changes ($\Delta F/F_0$) measured from small regions of interest ($1.3\ \mu\text{m} \times 1.3\ \mu\text{m}$) centered on the puff sites numbered in (A) and (B). The gray arrow indicates the time of the spot flash, and the open arrows mark the times of the first puff at each site. (D) Scatter plots show measurements of first-puff latencies from all sites in the two cells illustrated in (A) as a function of the distance of that site from the stationary spot flash (top) or from the lower end of the cell in the case of the distributed flash (bottom). Latencies are plotted on a logarithmic scale to better encompass the wide range of values.

from zero, whereas there was no significant distance dependence for distributed flash stimulation (fig. S1).

These experiments to determine puff latencies were performed with cells loaded with EGTA to suppress global Ca^{2+} waves. To verify that the stimulation conditions produced physiologically relevant IP_3 concentrations, we photoreleased equivalent amounts of i-IP_3 in cells that had not been loaded with EGTA (fig. S2). We observed global Ca^{2+} signals in 13 of 16 (81%), 16 of

21 (76%), and 19 of 19 (100%) cells stimulated with a distributed flash for 100, 200, and 500 ms, respectively. In parallel experiments in EGTA-loaded cells, the 200-ms flash evoked puffs with a mean latency of 6.3 s, closely matching that in the experiment shown in Fig. 2D. Therefore, the stimulus conditions were in a physiologically relevant range of IP_3 concentrations.

The data shown for the SH-SY5Y cells were obtained using the same culture of cells loaded under the same conditions to ensure internal consistency.

We observed similar results in two other experiments with SH-SY5Y cells and in one with COS-7 cells in which we measured 17 cells (fig. S3, A and B).

The overall mean latencies of puffs evoked by distributed flash stimulation decreased as the durations of the flash increased and, for each given flash duration, the distributions of puff latencies approximated exponential functions (Fig. 3A), consistent with previous findings (10). In contrast to the lack of spatial variation in puff latencies after distributed flash stimulation, the latency distributions of puffs evoked by a 500-ms spot flash stimulation varied with distance, with a time constant of ~ 1 s within $<15 \mu\text{m}$ of the spot and ~ 10 s at sites $>15 \mu\text{m}$ away (Fig. 3B).

Given that the latency to the first occurrence of a puff at a site is an inverse function of $[\text{IP}_3]$ (10), we interpreted the increasing first-puff latency at greater distances from the spot flash stimulation to arise from the time needed for i-IP_3 to diffuse along the length of the cell. To derive the diffusion rate of i-IP_3 in the cytosol, we needed to know how the latency varies with flash duration (amount of photoreleased i-IP_3) under our experimental conditions. To obtain this relationship, we plotted (Fig. 3C) the mean latencies of the first puffs evoked by distributed flash

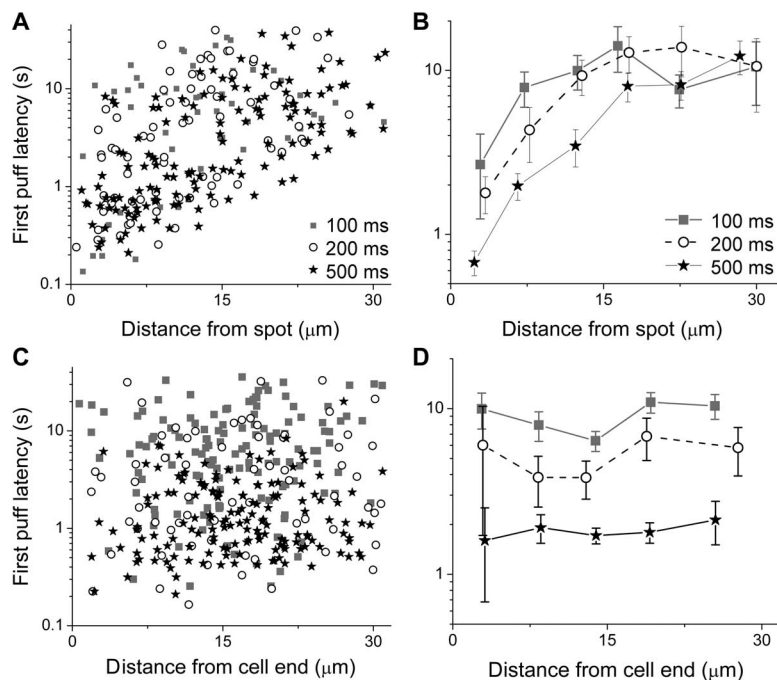


Fig. 2. First-puff latencies increase with increasing distance from spot flash photorelease of i-IP_3 but show no systematic variation with position along the cell for distributed flash photorelease of i-IP_3 . (A) Scatter plot showing first-puff latencies at individual puff sites after spot flash photorelease of i-IP_3 as a function of distance from the laser spot after flashes of 100-ms (gray squares, eight cells, 52 puff sites), 200-ms (open circles, seven cells, 75 puff sites), and 500-ms duration (stars, nine cells, 137 puff sites). The y axis is plotted on a logarithmic scale to better display the wide variability in observed puff latencies. (B) Mean measurements of first-puff latency obtained by binning the data in (A) in $\sim 5\text{-}\mu\text{m}$ increments. (C and D) Corresponding plots of individual (C) and mean binned puff latency data (D) after distributed flash photorelease of i-IP_3 . The spot flash intensity and total exposure times were the same as for the spot flash stimulation in (A) and (B). Data from the 100-, 200-, and 500-ms total exposure durations are from eight cells at 134 puff sites, eight cells at 76 sites, and seven cells at 152 sites, respectively. Error bars indicate \pm SEM.

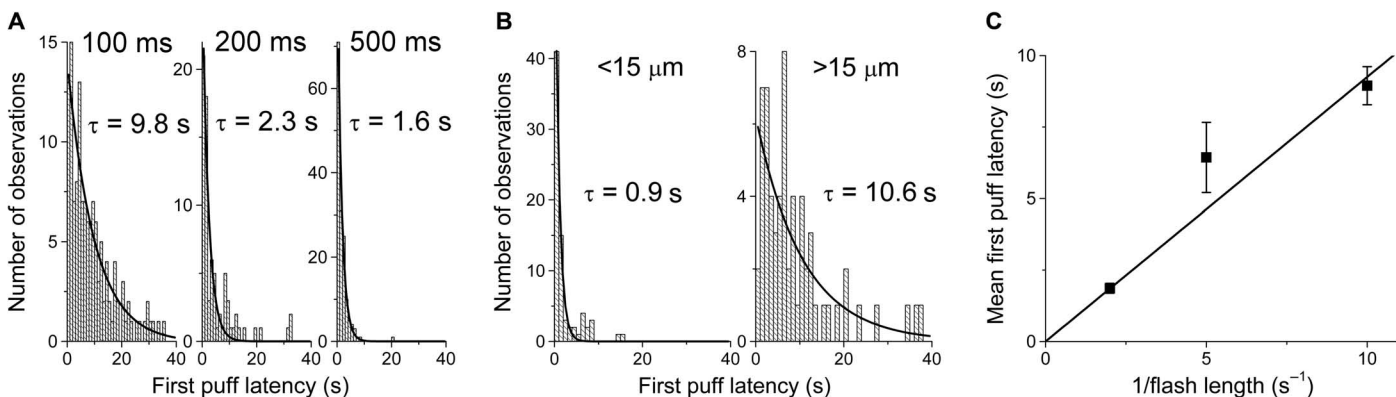


Fig. 3. Distributions of first-puff latencies and dependence of mean first-puff latency on photolysis flash duration. (A) Distributions of first-puff latencies evoked after distributed flash stimulation of i-IP_3 with the indicated total flash durations. (B) Distributions of first-puff latencies after a 500-ms spot flash stimulation at sites within (left) and beyond (right) $15 \mu\text{m}$ of the laser spot. Data in (A) and (B) are fitted by single-exponential functions, with time constants τ as indicated. (C) Mean first-puff latency after distributed flash stimulation of i-IP_3 plotted as a function of reciprocal flash duration. Error bars indicate \pm SEM and are smaller than the symbol width for the leftmost point. The data are fitted by a regression line, constrained to the origin, with a slope of 0.90.

stimulation as a function of reciprocal flash duration, which is a linearly proportional measure of the amount of photoreleased $i\text{-IP}_3$, assuming that only a small fraction of the total caged $i\text{-IP}_3$ was released by photolysis (15). Concordant with previous findings (10), the data fit to a linear relationship, with the latency shortening in direct proportion to increasing $[i\text{-IP}_3]$. Using the slope of the relationship (0.90 ± 0.05 in units relative to flash duration), we constructed a model of the predicted distribution of puff latencies as $i\text{-IP}_3$ diffused through the cell.

Simulation of IP_3 diffusion and puff triggering

To obtain a quantitative estimate of the effective diffusion coefficient of IP_3 , we compared our experimental data of first-puff latencies with predictions obtained by model simulations of the diffusion equation using various diffusion coefficients (methods S1). We used a simplified, closed-end, one-dimensional model, representing the average length of cells used in the experiments ($40 \mu\text{m}$; fig. S4A). In the model, we introduced IP_3 at the spot flash stimulation site in relative amounts corresponding to the different flash durations, over a time course matching the flash duration and with a spatial distribution approximating that of the UV laser spot (fig. S4B). After the introduction of IP_3 , we assumed that the total amount remained constant, mimicking the slow degradation of $i\text{-IP}_3$ in the cytosol (3, 4).

Heat maps of simulated spatiotemporal profiles of IP_3 concentration resulting from a modeled 500-ms flash illustrate the different results obtained with two effective diffusion coefficients: $10 \mu\text{m}^2 \text{s}^{-1}$ (Fig. 4A) and $280 \mu\text{m}^2 \text{s}^{-1}$, the value obtained by Allbritton *et al.* (1) (Fig. 4B). From these simulation results, we plotted the change in IP_3 concentrations over time at select distances along the modeled cells with the different

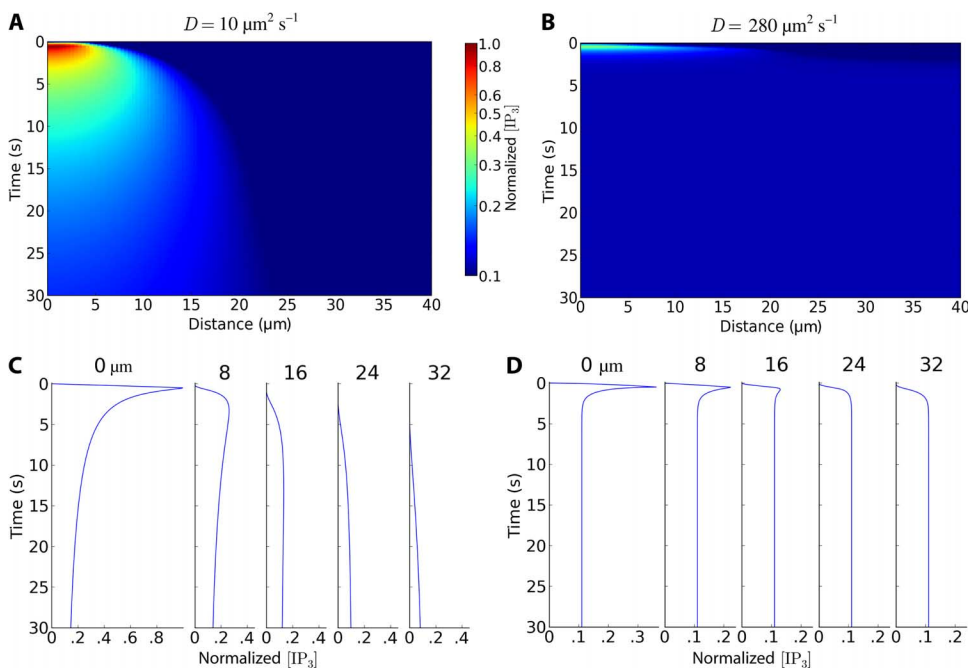


Fig. 4. Simulation of IP_3 diffusion after spot flash stimulation. Panels illustrate the simulated diffusion of IP_3 in a $40\text{-}\mu\text{m}$ -long, one-dimensional model of a cell after spot (Gaussian profile with $\sigma = 1.35 \mu\text{m}$) flash stimulation at one end with a flash duration of 500 ms. After the flash, the total amount of IP_3 was conserved through the cell (no degradation occurred). The diffusion coefficients used in the simulations are indicated at the top. **(A and B)** Heat maps representing IP_3 concentrations at different times (y axis, with time running from top to bottom) and distances (x axis) after the beginning of the flash at time 0. IP_3 concentrations are in arbitrary units but are consistent for both panels. **(C and D)** Temporal profiles of $[\text{IP}_3]$ at different distances (indicated in μm) along the modeled cell. Concentrations of IP_3 in both panels are expressed normalized to the peak concentration attained at the photolysis spot site for $D = 10 \mu\text{m}^2 \text{s}^{-1}$.

diffusion constants (Fig. 4, C and D). When the diffusion coefficient was set to $280 \mu\text{m}^2 \text{s}^{-1}$, the IP_3 concentration equilibrated across the cell within about 1 s to a final normalized concentration of ~ 0.11 . For a diffusion coefficient of $10 \mu\text{m}^2 \text{s}^{-1}$, the local concentration of IP_3 in the vicinity of the modeled spot flash remained considerably greater than the final equilibrium concentration for several seconds, whereas the concentration at the distal end of the cell did not begin to increase appreciably for more than 5 s and was still below the equilibrium level after as long as 20 s.

We used these predicted spatiotemporal concentration profiles to compute the probability of observing a puff at each position along the length of the one-dimensional cell at any given time after the introduction of IP_3 (onset of the spot flash; methods S1). For each spatial element and time point in the model, we calculated the puff-triggering rate that corresponded to the instantaneous concentration of IP_3 predicted by the simulations in Fig. 4 using the slope value from Fig. 3C, in which a distributed flash photorelease of IP_3 evoked first puffs at a rate (inverse mean latency) of 1.11s^{-1} per second of flash duration. The heat maps of the predicted puff-triggering rates for IP_3 diffusion coefficients of 10 and $280 \mu\text{m}^2 \text{s}^{-1}$ showed different probability patterns (Fig. 5, A and B). From these simulation results, we derived the corresponding probabilities of observing an initial puff at select distances along the modeled cell as a function of time, taking into account the increasing chance that a puff would have already occurred during previous time points (Fig. 5, C and D). Finally, we computed how the first-puff latencies varied with distance from the spot where IP_3 was introduced (the simulated spot flash stimulation) for a 500-ms spot flash duration and respective diffusion coefficients of 10 and $280 \mu\text{m}^2 \text{s}^{-1}$ (Fig. 5, E and F, blue curves).

In the case of the $280 \mu\text{m}^2 \text{s}^{-1}$ diffusion coefficient, almost all first puffs were predicted to arise within 5 s of the introduction of IP_3 (Fig. 5D), and there was only a small dependence of first-puff latencies on distance from the introduction spot, increasing from about 1.5 s at the introduction site to about 2.5 s at the far end of the modeled cell (Fig. 5F). These predicted values are close to the experimental measurements obtained with distributed flash stimulation across the cell (indicated by the red line in Fig. 5F), concordant with a rapid spatial equilibration of IP_3 . In marked contrast, simulations with a diffusion coefficient of $10 \mu\text{m}^2 \text{s}^{-1}$ showed large differences in puff latency distributions with distance (Fig. 5C). Mean latencies near the IP_3 introduction site (~ 0.4 s) were shorter than those measured after distributed introduction of the same amount of IP_3 (red line), whereas they lengthened to ~ 11 s at the end of the modeled cell farthest from the site of IP_3 introduction (Fig. 5E).

Estimating the IP_3 diffusion coefficient by fitting simulated to experimental data

The simulation results indicated that using a diffusion coefficient of $10 \mu\text{m}^2 \text{s}^{-1}$ better matched our experimental results

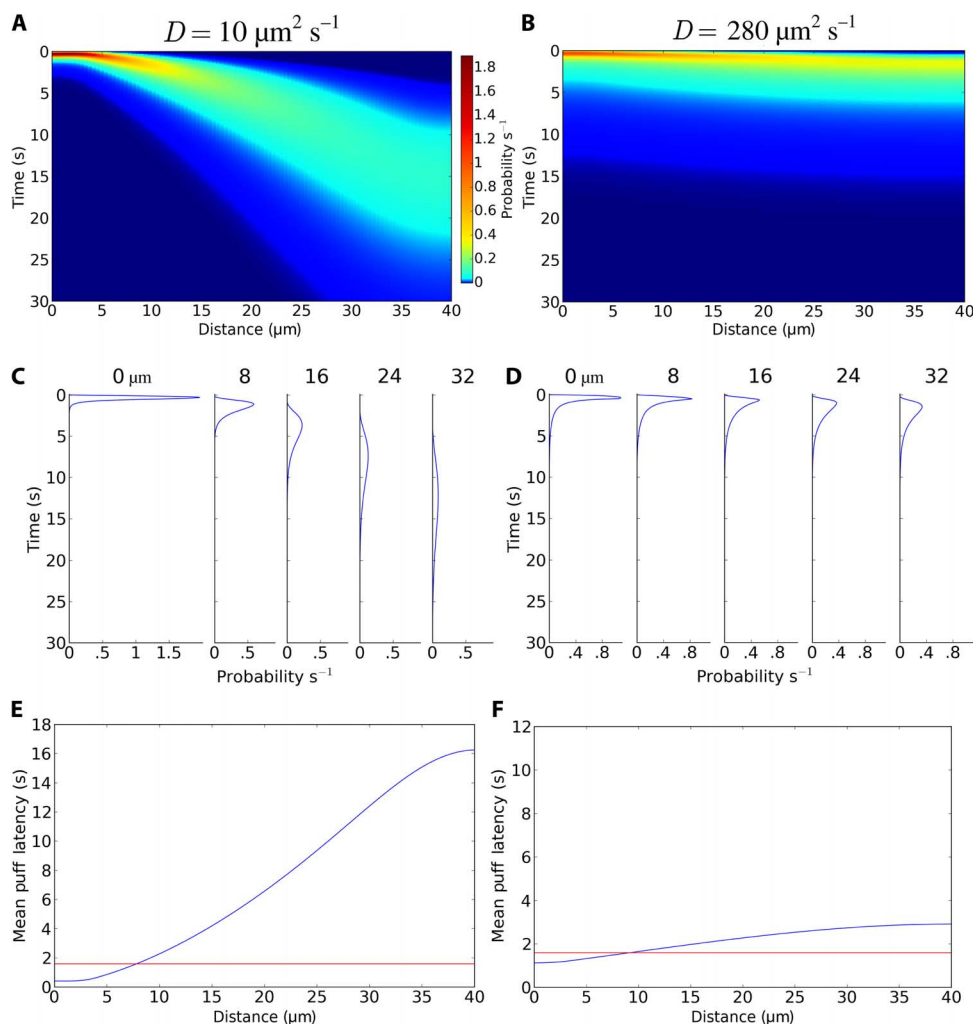


Fig. 5. Simulation of the probability of observing puffs at different times and distances after spot photorelease of IP₃. Simulations were based on the spatiotemporal concentration profiles in Fig. 4, assuming that the probability of puff triggering is a linear function of [IP₃]. The diffusion coefficients used in the simulations are indicated at the top. **(A and B)** Heat maps representing the probability of observing a puff at different times (y axis, with time running from top to bottom) and distances along the cell (x axis) after the beginning of the flash at time 0. **(C and D)** Temporal profiles of puff probability at different distances (indicated in μm) along the cell. **(E and F)** Predicted mean latencies of puffs as a function of distance along the cell from the flash. Horizontal lines indicate the mean puff latency if the same total amount of IP₃ were released uniformly along the cell by distributed flash stimulation.

than a diffusion coefficient of 280 μm² s⁻¹. To refine our estimate of the IP₃ diffusion coefficient, we performed additional simulations using a range of diffusion coefficients between 1 and 280 μm² s⁻¹. Simulations were performed by calculating the probabilities of puff occurrence within 30 s of IP₃ introduction (mimicking the experimental recording time for the response to spot flash stimulation of i-IP₃). This procedure normalizes the comparison between experimental and simulated data by accounting for missed long-latency puffs that may have occurred after the end of recordings (see methods S1).

Superimposition of the experimental data corresponding to spot flash stimulation for 500 ms (Fig. 2B) with the predicted mean first-puff latencies, as a function of distance from a 500-ms duration introduction of IP₃, showed that the experimental data matched best with the simulation curves generated with diffusion constants of 5 or 10 μm² s⁻¹ (Fig. 6A). Plotting the experimental data together with the simulation

curves for all flash durations further indicated that a diffusion coefficient of 280 μm² s⁻¹ would not match the data well (fig. S5). We quantified the goodness of fit to the simulated relationships by calculating the mean squared differences between experimental and simulated data for different values of IP₃ diffusion coefficients (Fig. 6B). For each flash duration and selected diffusion coefficient, the mean squared error is the average of the squared differences between the binned mean observed latencies (Fig. 6A and fig. S5) and the predicted mean latencies at the corresponding distances. This analysis showed that the minimum values (representing the best fit) were obtained with diffusion coefficients between 3 and 10 μm² s⁻¹, with the best-fit diffusion coefficient tending to higher values with increasing flash duration.

We did not apply this model to estimate a diffusion coefficient for IP₃ in COS-7 cells because their more complex morphology cannot be approximated as a one-dimensional situation. Nevertheless, the observed about threefold lengthening of mean puff latency over a 20-μm distance from the spot flash stimulation site indicates that diffusion of IP₃ is strongly hindered in COS-7 cells (fig. S3B). If IP₃ were to diffuse freely with a diffusion coefficient of 280 μm² s⁻¹, its concentration would equilibrate over this distance within <1 s, so puff latencies would show little or no apparent dependence on distance.

Range of action of IP₃

Allbritton *et al.* (1) defined the range of action of a messenger as

$$\sqrt{2D\tau} \tag{1}$$

where D is the effective diffusion coefficient of the messenger and τ is its mean lifetime before degradation. This expression represents an equilibrium value and does not take into account the time it takes a messenger to diffuse from a localized source. In light of our observations of slow diffusion of IP₃, we propose a redefinition of the range of action as (see methods S2)

$$\text{range of action} = \frac{\int_0^\infty x\Phi_T(x)dx}{\Phi_T(x)dx} \tag{2}$$

$$\Phi_T(x) \stackrel{\text{def}}{=} \int_0^T [\text{IP}_3]_{D,\tau}(x,t)dt \tag{3}$$

where x is the distance from the IP₃ source, T is any given time (t) after deposition of the messenger, and $[\text{IP}_3]_{D,\tau}(x,t)$ is the IP₃ concentration

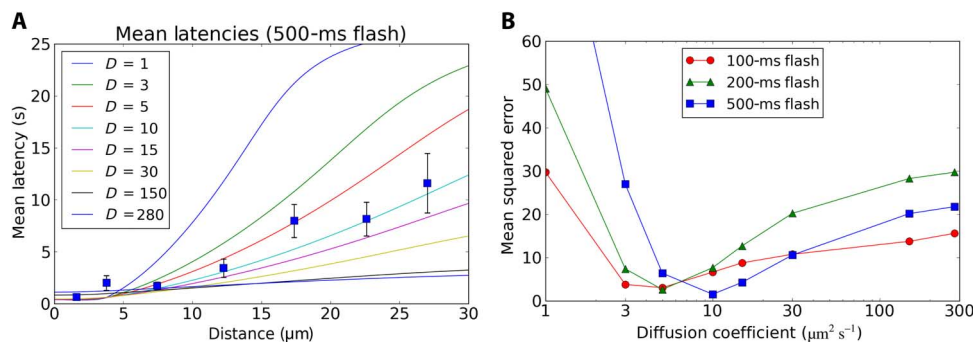


Fig. 6. Comparison of experimental with simulated data indicates an effective intracellular diffusion coefficient for IP_3 of 3 to $10 \mu m^2 s^{-1}$. (A) Comparison of experimental and predicted first-puff latencies evoked by a 500-ms spot flash stimulation. Curves plot the predicted mean first-puff latencies as a function of distance along the cell from the stationary photolysis spot for various values of IP_3 diffusion coefficient, as indicated in units of $\mu m^2 s^{-1}$. Data points show mean \pm SEM of first-puff latencies from the experiment shown in Fig. 2 (A and B). (B) Mean squared error between observed and predicted puff latencies as a function of the simulated IP_3 diffusion coefficient. Curves are shown for experimental and simulated data for flash durations of 100, 200, and 500 ms.

that results from diffusion with effective coefficient D and mean lifetime τ . Intuitively, this can be considered as the distance from a point source over which one-half of the total cumulative actions of the messenger would have occurred (Fig. 7, A and B). Our definition also corresponds to the median distance over which a messenger that is continuously deposited in the one-dimensional model cell at position $x = 0$ is spread when a time T has elapsed since deposition was initiated (16). In a biological cell, the messenger would be produced (“deposited”) in response to a signal and then its range of action would be dictated by both its degradation and diffusion. Heat maps illustrate the range of action predicted by Eq. 2 as a function of effective diffusion coefficient and degradation rate, calculated for 0.1, 1, 10, and 100 s after an instantaneous appearance of the messenger (Fig. 7, C to F). These heat maps showed that the range of action over short intervals (≤ 1 s) is narrowly restricted ($< 5 \mu m$) and dominated by the diffusion coefficient (Fig. 7, C and D), whereas at longer intervals, the range of action becomes more extended and is dependent on both the diffusion coefficient and the rate of degradation of the messenger (Fig. 7, E and F).

DISCUSSION

Intracellular diffusion and range of action of IP_3

We investigated the diffusion of IP_3 in neuroblastoma cells by locally photoreleasing a poorly metabolized IP_3 analog at one end of these elongated cells and monitoring its subsequent spread by the timing of discrete IP_3 -evoked, Ca^{2+} release events (puffs) at multiple sites along the cell. Using the first-puff latency as an endogenous reporter of local $[IP_3]$, we obtained estimates of the effective diffusion coefficient of IP_3 in the cytoplasm of intact mammalian cells under physiologically relevant IP_3 concentrations, with minimal perturbation of cellular function and structure.

By comparing our experimental puff latency data to predicted puff-triggering probabilities in a one-dimensional model, we obtained the best agreement for an effective diffusion coefficient D of ~ 3 to $10 \mu m^2 s^{-1}$ for IP_3 . Although our model does not fully replicate the complex three-dimensional cellular architecture, we selected relatively elongated cells for study. Another possible source of error is that basal Ca^{2+} concentrations were not fully clamped by the EGTA loaded into the cells, so puff triggering may have been accelerated by a slow, progressive increase in basal free cytosolic $[Ca^{2+}]$ (Fig. 1C). This increase in

basal $[Ca^{2+}]$ would have the most pronounced effect at sites distant from the photolysis spot where puff latencies were long, with a potential net effect that our values for the IP_3 diffusion coefficient are overestimated.

The effective diffusion coefficient of IP_3 that we determined is ~ 30 -fold slower than the value ($283 \pm 53 \mu m^2 s^{-1}$) reported by Allbritton *et al.* (1). The larger value has become widely accepted (17–20), leading to the conclusion that the range of action of IP_3 is sufficiently large that it functions as a global messenger in mammalian cells of typical size (1, 2). Published values for the half-life (τ) of IP_3 in cells range widely from one to several seconds in mammalian cells (2), including 10 to 20 s in neuroblastoma cells (11, 21) to a minute or more in *Xenopus*

oocytes (2, 21). Defining the range of action as in Eq. 1 and assuming that $D = 280 \mu m^2 s^{-1}$ and $\tau = 1$ s, Allbritton *et al.* (1) obtained a range of action of about $25 \mu m$. However, taking our value of the effective diffusion coefficient $D = 3$ to $10 \mu m^2 s^{-1}$, the range is reduced to $< 5 \mu m$, indicating that IP_3 should no longer be considered a global messenger and that appreciable spatial gradients of IP_3 may arise within even small cells. The range of action of IP_3 is comparable to that ($\sim 5 \mu m$) for the buffered diffusion of Ca^{2+} (1, 13), which is considered a local messenger.

Physiological implications of hindered diffusion of IP_3

The restricted effective diffusion of IP_3 likely has important physiological implications for IP_3 -mediated signaling. Ca^{2+} release from the endoplasmic reticulum (ER) through IP_3 R requires binding of both cytosolic IP_3 and Ca^{2+} to receptor sites on the tetrameric IP_3 R, leading to a regenerative process of Ca^{2+} -induced Ca^{2+} release (22). This process can support the generation of propagating Ca^{2+} waves by a fire-diffuse-fire model (23), wherein Ca^{2+} released through IP_3 R at one site diffuses to activate release through surrounding IP_3 -bound IP_3 R. Thus, although Ca^{2+} wave propagation can be considered to overcome the limited effective diffusional range of Ca^{2+} ions, the extent to which a Ca^{2+} wave can propagate is set by the diffusional spread of IP_3 , if IP_3 is generated from a localized source. The impact of the diffusional spread will be particularly strong in extended cellular processes, such as neuronal dendrites, and in the propagation of intercellular Ca^{2+} signals mediated by the diffusion of IP_3 through gap junctions (24, 25).

The expression (Eq. 1) for the range of action as formulated by Allbritton *et al.* (1) does not adequately describe many physiological situations. If the messenger is not degraded, its range of action goes to infinity. Furthermore, the range of action given by Eq. 1 does not take time into account. Our data provide a clear example of these limitations, in that Ca^{2+} signals at the distal end of the cell arose after latencies ~ 10 -fold longer than those near the site of photoreleased IP_3 , even though degradation of $i-IP_3$ was negligible (11). Timing is crucial for many physiological processes—it is not merely the final concentration to which a diffusible messenger ultimately increases but how quickly it increases and subsequently decreases is also critical for shaping the cellular response to the messenger. In place of the Allbritton *et al.* expression, we thus propose a more biologically relevant expression (Eq. 2),

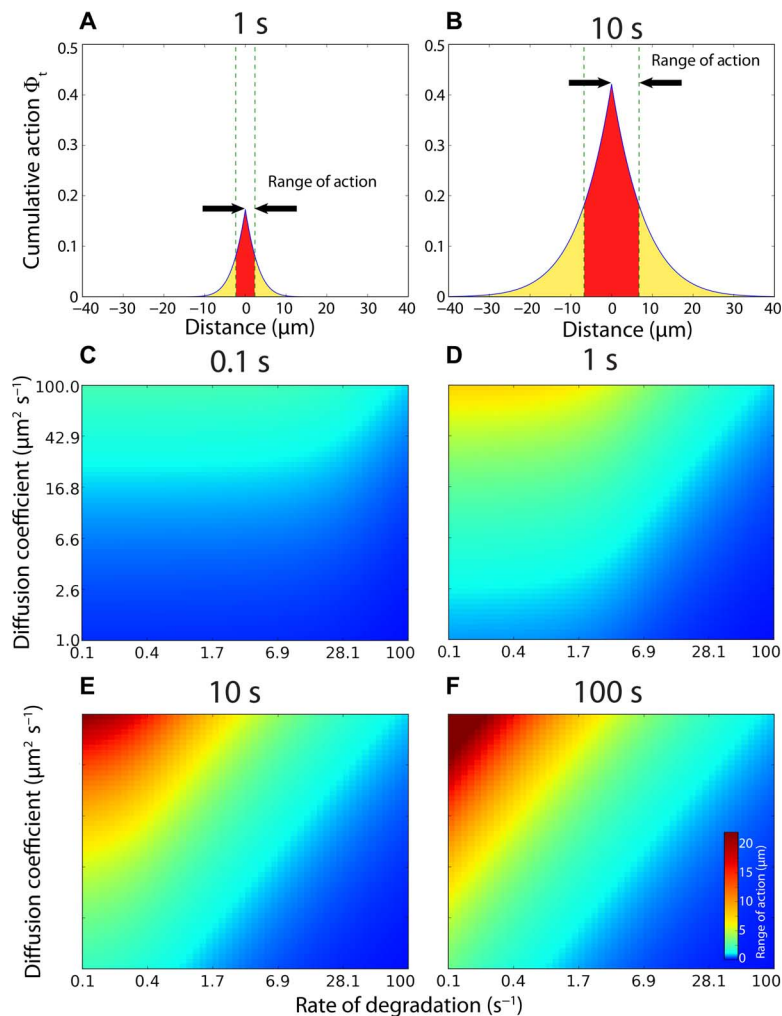


Fig. 7. Time dependence of the range of action of an intracellular messenger. We define the range of action at a given time T as the distance from a transient point source of messenger at which half of its total cumulative actions (given by Eq. 2) will have occurred. (A and B) Illustrations showing the range of action after times $T = 1\text{ s}$ (A) and 10 s (B) for a diffusion coefficient $D = 10\text{ }\mu\text{m}^2\text{ s}^{-1}$ and mean messenger lifetime $\tau = 10\text{ s}$. The schematic represents a one-dimensional model cell extending infinitely far on each side from a transient, point source of messenger; the profile and range of action are identical for a one-sided model extending infinitely from a closed end where the messenger is introduced. The y axis is in arbitrary units. (C to F) Heat maps showing the predicted ranges of action of an intracellular messenger at times $T = 0.1\text{ s}$ (C), 1 s (D), 10 s (E), and 100 s (F) for different combinations of effective diffusion coefficient and rate of degradation (inverse mean lifetime) of the messenger.

equating the range of action as the distance from the source over which one-half of the total cumulative actions of the messenger would have occurred at any given time (Fig. 7, A and B) (methods S2). Using our expression for range of action, at long times ($t \gg \tau$) after the appearance of the messenger, the expression converges to $\sqrt{D\tau}$, which yields a range of action shorter by a factor of $\sqrt{2}$ than the range given by the Allbritton *et al.* expression. For example, for $D = 10\text{ }\mu\text{m}^2\text{ s}^{-1}$ and $\tau = 1\text{ s}$, the steady-state range of action given by our expression is ~ 3.3 and that given by the Allbritton *et al.* expression is $\sim 4.5\text{ }\mu\text{m}$. Potentially of more biological importance, Eq. 2 indicates that for short times ($t < \tau$), the range of action becomes increasingly independent of messenger degradation and varies approximately as a square root function of time. Considering the same example, the predicted range of action is further reduced to $1.60\text{ }\mu\text{m}$ over an interval of 500 ms after the introduction of messenger.

membrane is low with a diffusion coefficient of $< 0.1\text{ }\mu\text{m}^2\text{ s}^{-1}$ (6), so they can be considered as immobile on the time and distance scales of our experiments. Binding to stationary, unoccupied receptor sites is thus expected to slow the effective diffusion of IP_3 in a manner analogous to the slowing of the diffusion of Ca^{2+} ions by binding to immobile cytoplasmic buffers. The ability of IP_3Rs to buffer IP_3 and slow its effective diffusion will diminish at increasing concentrations of IP_3 because an increasing fraction of the binding sites becomes occupied. Our results showed a trend for the effective diffusion coefficient to increase from about 3 to $10\text{ }\mu\text{m}^2\text{ s}^{-1}$ over the fivefold range of photo-released $i\text{-IP}_3$ that we explored. We anticipate that the released $i\text{-IP}_3$ represents a physiological range of IP_3 concentrations because even the weakest photolysis flash evoked robust global Ca^{2+} waves in cells not loaded with EGTA (fig. S2).

This dependence on IP_3 metabolism may be of particular importance for IP_3 signaling in neurons, where the dual gating of IP_3 receptors by IP_3 and cytosolic Ca^{2+} has been proposed to function as a coincidence detector. Specifically, the ability of IP_3 to evoke intracellular Ca^{2+} release as it diffuses along a dendrite after local metabotropic receptor activation at one site may be promoted by a subsequent action potential that evokes entry of Ca^{2+} through plasma membrane channels (26, 27) or by summation with local production of IP_3 (28) at other sites further along the dendrite. A lower effective diffusion coefficient of IP_3 would narrow the spatiotemporal window over which the coincidence of these signals would occur because the spread of IP_3 would be more restricted, and IP_3 concentrations at distant sites may rise too slowly to coincide with the increase in Ca^{2+} .

Hindered diffusion of IP_3 by binding to silent IP_3Rs

What might underlie the markedly hindered diffusion of IP_3 in neuroblastoma cells, and why does this markedly differ from the free mobility of IP_3 reported by Allbritton *et al.* in oocyte cytoplasmic extracts? The slow intracellular diffusion of IP_3 in the cytosol cannot readily be explained by nonspecific factors, such as tortuosity or viscosity, given that the diffusion coefficient of adenosine 5'-triphosphate (ATP)—a molecule of similar size and identical charge to IP_3 —is only slightly lower in cells than in free solution [248 and $349\text{ }\mu\text{m}^2\text{ s}^{-1}$, respectively (29)]. Instead, we propose that diffusion of IP_3 is limited by binding to the large number of IP_3Rs estimated to be present in SH-SY5Y and other mammalian cells (5). The motility of IP_3Rs in the ER

Concordant with a mechanism of physiological IP₃ buffering, Finch and Augustine (30) observed that Ca²⁺ signals evoked by spot photorelease of IP₃ (not the poorly metabolized i-IP₃ analog) in the dendrites of cerebellar Purkinje cells were restricted to a few micrometers, a finding that they interpreted to result from binding to the high density of IP₃Rs in these cells. In contrast, the experiments of Allbritton *et al.* (1) were made using cytosolic extracts from *Xenopus* oocytes in which IP₃Rs are concentrated in a thin circumferential shell around these giant cells (31, 32). The concentration of IP₃Rs in these extracts would have been diluted by the large bulk of cytoplasm from the oocyte interior. Moreover, binding to receptor sites may have been saturated by the concentration of radiolabeled IP₃ (100 nM total IP₃) applied to monitor diffusion. In this context, we therefore believe that the *Xenopus* oocyte cytoplasm does not serve well as a model system for small mammalian cells.

The calculated diffusion coefficient for IP₃ in a medium with twice the viscosity of water is about 250 μm² s⁻¹ (1), similar to the measured value for ATP in cells (29). We interpret our finding of an effective diffusion coefficient of ≤10 μm² s⁻¹ as arising because specific binding of IP₃ to immobile sites slows its effective diffusion by a factor of ≥25. Assuming that binding equilibrates rapidly and that only a small fraction of all sites are bound, the effective diffusion coefficient D_{eff} is given by

$$D_{\text{eff}} = \frac{D}{1 + R} \quad (4)$$

where D is the diffusion coefficient in the absence of binding and R is the ratio of concentration of binding sites to the dissociation constant K_d of binding to these sites (33). Our results thus lead to an R value of ≥24. This differs markedly from the value of ~1 calculated from the intracellular IP₃R concentration of 100 nM and a K_d of 113 nM reported by Taylor and Konieczny (5) and Ding *et al.* (34). With an R of 1, the effective diffusion coefficient of IP₃ would be reduced by no more than a factor of 2 from that in the absence of binding.

Silent and functional IP₃Rs

Ca²⁺ puffs involve the concerted opening of several IP₃Rs, tightly clustered at immobile, sparsely distributed sites throughout the cell (3, 4). A long-standing question is why Ca²⁺ release is restricted to these specific sites, involving only about 3% of the total number of IP₃Rs in the cell, whereas the great majority of IP₃Rs appear functionally silent under the same conditions even though the slow diffusion of IP₃ suggests that they bind IP₃ (5, 35).

Our results, considered together with evidence that the tetrameric IP₃R channel requires IP₃ to be bound to all four receptor sites before it can be activated (5, 36), cast light on this issue. The hindered diffusion of IP₃ and the relative insensitivity of the effective diffusion coefficient to changes in the amount of photoreleased IP₃ (from ~3 μm² s⁻¹ with a 100-ms flash to ~10 μm² s⁻¹ with a 500-ms flash) indicated that a substantial fraction of binding sites must remain unoccupied. How then can Ca²⁺ puffs be generated under these conditions, given that they involve the concerted opening of several, tightly clustered IP₃Rs (3, 4)? As an example, for a cluster of four channels, the probability that all will be available to open during a puff increases as the 16th power of [IP₃] increases, so a concentration that yields a 50% probability that all four IP₃Rs are activated (binding four IP₃ molecules) corresponds to an overall occupancy of receptor sites of 95.8%. It seems that the IP₃Rs active at puff sites must be functionally different from the silent receptors that hinder binding, in addition to their differing spatial localization and

motility (5, 6, 35). The mechanism remains unknown, but possibilities include that receptors at puff sites exhibit a much higher affinity of IP₃ binding or that their gating properties are modified so that channel opening requires binding of fewer than four IP₃ molecules per tetramer.

MATERIALS AND METHODS

Reagents

Unless otherwise indicated, all reagents were obtained from Sigma, and cell culture media were from Invitrogen.

Cell culture

SH-SY5Y human neuroblastoma cells were cultured as previously described (4) in a 1:1 mix of Ham's F12 medium and Eagle's minimum essential medium, supplemented with fetal calf serum [10% (v/v)], non-essential amino acids [1% (v/v)], and penicillin-streptomycin [1% (v/v)]. Cells were incubated at 37°C in a humidified incubator with 95% air and 5% CO₂ and were passaged every 2 to 3 days to a maximum of 20 passages. Four days before imaging, cells were harvested in Ca²⁺/Mg²⁺-free phosphate-buffered saline (pH 7.4) and cultured on glass coverslips in petri dishes (35-mm dish, no. 1.0 coverglass; MatTek) at a density of ~3 × 10⁴ cells/ml. On the day of imaging, cells were washed in Hepes-buffered saline solution [HBS; composition: 135 mM NaCl, 5 mM KCl, 1.2 mM MgCl₂, 2.5 mM CaCl₂, 5 mM Hepes, and 10 mM glucose (pH 7.4)].

Ca²⁺ imaging and localized photorelease of i-IP₃

Cultured SH-SY5Y cells were loaded for imaging by incubation with membrane-permeant esters of Fluo-4 (1 μM; Invitrogen), EGTA (5 μM; Invitrogen), and caged i-IP₃ (1 μM; SiChem) in HBS, as described (4). Cells averaged ~40 μm in length along the cell body (fig. S4A). Cytosolic Ca²⁺ changes were imaged using a total internal reflection fluorescence (TIRF) microscope system (4) constructed around an Olympus IX70 microscope with a 60× TIRF objective (numerical aperture, 1.45). Fluo-4 fluorescence was excited by 488-nm laser light within an evanescent field extending a few hundred nanometers into the cells, and emitted fluorescence (λ > 510 nm) was imaged at a resolution of 256 × 256 pixels (1 pixel = 0.266 μm) at an exposure time of 15 ms (~66 frames s⁻¹) using the center quad of an Evolve 512 electron-multiplying charge-coupled device camera (Roper Scientific). Image data were acquired as stack files using MetaMorph v7.7 (Universal Imaging/Molecular Devices) and were analyzed offline to detect the locations of puff sites and to measure puff latencies. The custom software used for analysis is described in and available from the work of Ellefsen *et al.* (14). Measurements were exported to Microcal Origin v8.0 (OriginLab) for analysis and graphing. Unless otherwise noted, data are presented as means ± 1 SEM.

Photorelease of i-IP₃

Photolysis of caged i-IP₃ was evoked by a custom-built system using computer-controlled galvanometer mirrors to direct light from a 405-nm laser diode module. The laser light was focused to a spot in the specimen (fig. S4B), which could be steered to any desired location within the imaging field using dim light from a coaxial 450-nm laser as a "guide star" to excite fluorescence in Fluo-4-loaded cells without causing photorelease of i-IP₃. A computer-generated TTL (transistor-transistor logic) signal controlled the duration of the 405-nm photolysis spot flash, and a variable neutral density filter wheel controlled its intensity. Experiments were performed using photolysis flashes of given duration and fixed intensity, with the laser spot either remaining stationary at one end of a cell to evoke localized photorelease of i-IP₃ (spot flash) or scanned along

the length of a cell during the same flash duration to evoke a spatially distributed photorelease (distributed flash). In the latter case, a line was defined by clicking the computer mouse after positioning the guide laser spot at each end of the cell, and the computer then stepped the 405-nm laser spot in 10 equal increments along the line during the flash duration. For example, a 100-ms flash would be delivered as 10 exposures, each with a 10-ms duration, spaced at 4- μm increments along a cell 40 μm in length. Given that flash durations were short (100 to 500 ms) in comparison to puff latencies, this distributed flash protocol leads to an approximately uniform photorelease of $i\text{-IP}_3$ throughout the cell, in an amount equivalent to that photoreleased by a stationary spot flash of the same duration and intensity.

Analytical derivation and numerical simulation of puff latencies

To simulate the diffusion of IP_3 and subsequent triggering of initial puffs after spot flash stimulation, we applied a simplified one-dimensional model. Analytical solutions of the model are presented in methods S1. To generate model data with which to fit to experimental observations, we performed numerical simulations of these solutions. The cell was represented as a 40- μm -long array, with closed ends, composed of 100 elements, each containing a single puff site. To simulate uncaging of IP_3 , we increased the concentration of IP_3 to a fixed amount for every time step during the duration of the photolysis flash. The spatial profile of uncaging was simulated as a Gaussian curve with a width ($\sigma = 1.35 \mu\text{m}$) corresponding to that of the UV laser spot. Because $i\text{-IP}_3$ is metabolically degraded more slowly than endogenous IP_3 , the rate of metabolism was set to 0, except where otherwise noted; that is to say, the total amount of IP_3 remained constant after the uncaging period. To then simulate the probability of a puff being triggered at each spatial element, we assumed a linear relationship between $[\text{IP}_3]$ and puff triggering (10), with a rate constant (1.11 s^{-1} per 1 s flash duration) derived from experiments (Fig. 3C), in which corresponding amounts of $i\text{-IP}_3$ were photoreleased uniformly throughout cells by the distributed flash protocol. For each spatial element, we then took the triggering rate as given by the concentration of IP_3 at a given time step and calculated the probability of observing the first puff at that site over successive time steps. Simulations were terminated after 30 s to match the duration of experimental recordings, and calculations of mean first-puff latencies were made only over this interval. Thus, mean values from both experimental and simulated data were unaffected by “missed” sites that failed to show a puff within 30s.

SUPPLEMENTARY MATERIALS

www.sciencesignaling.org/cgi/content/full/9/453/ra108/DC1

Methods S1. Theoretical derivation of puff latencies

Methods S2. Calculation of range of action

Fig. S1. First-puff latencies depended strongly on the distance from the spot flash stimulation, whereas there was no significant distance dependence for distributed flash stimulation.

Fig. S2. Ca^{2+} waves evoked by photoreleased $i\text{-IP}_3$ in SH-SY5Y cells without EGTA.

Fig. S3. Latencies of puffs evoked by spot photorelease of $i\text{-IP}_3$ in COS-7 cells.

Fig. S4. Lengths of SH-SY5Y cells and spatial extent of the photolysis laser spot.

Fig. S5. Experimental and simulated first-puff latency data for the 100- and 200-ms spot flash durations.

Movie S1. Puffs evoked by localized and distributed flash photorelease of IP_3 .

Reference (37)

REFERENCES AND NOTES

- N. L. Allbritton, T. Meyer, L. Stryer, Range of messenger action of calcium ion and inositol 1,4,5-trisphosphate. *Science* **258**, 1812–1815 (1992).
- C. E. Sims, N. L. Allbritton, Metabolism of inositol 1,4,5-trisphosphate and inositol 1,3,4,5-tetrakisphosphate by the oocytes of *Xenopus laevis*. *J. Biol. Chem.* **273**, 4052–4058 (1998).
- I. F. Smith, S. M. Wiltgen, J. Shuai, I. Parker, Ca^{2+} puffs originate from preestablished stable clusters of inositol trisphosphate receptors. *Sci. Signal.* **2**, ra77 (2009).
- I. F. Smith, I. Parker, Imaging the quantal substructure of single IP_3R channel activity during Ca^{2+} puffs in intact mammalian cells. *Proc. Natl. Acad. Sci. U.S.A.* **106**, 6404–6409 (2009).
- C. W. Taylor, V. Konieczny, IP_3 receptors: Take four IP_3 to open. *Sci. Signal.* **9**, pe1 (2016).
- I. F. Smith, D. Swaminathan, G. D. Dickinson, I. Parker, Single-molecule tracking of inositol trisphosphate receptors reveals different motilities and distributions. *Biophys. J.* **107**, 834–845 (2014).
- B. S. Wilson, J. R. Pfeiffer, A. J. Smith, J. M. Oliver, J. A. Oberdorf, R. J. H. Wojcikiewicz, Calcium-dependent clustering of inositol 1,4,5-trisphosphate receptors. *Mol. Biol. Cell* **9**, 1465–1478 (1998).
- S. C. Tovey, P. de Smet, P. Lipp, D. Thomas, K. W. Young, L. Missiaen, H. De Smedt, J. B. Parys, M. J. Berridge, J. Thuring, A. Holmes, M. D. Bootman, Calcium puffs are generic InsP_3 -activated elementary calcium signals and are downregulated by prolonged hormonal stimulation to inhibit cellular calcium responses. *J. Cell Sci.* **114**, 3979–3989 (2001).
- Y. Yao, J. Choi, I. Parker, Quantal puffs of intracellular Ca^{2+} evoked by inositol trisphosphate in *Xenopus* oocytes. *J. Physiol.* **482**, 533–553 (1995).
- G. D. Dickinson, D. Swaminathan, I. Parker, The probability of triggering calcium puffs is linearly related to the number of inositol trisphosphate receptors in a cluster. *Biophys. J.* **102**, 1826–1836 (2012).
- K. Dakin, W.-H. Li, Cell membrane permeable esters of *D*-myo-inositol 1,4,5-trisphosphate. *Cell Calcium* **42**, 291–301 (2007).
- I. F. Smith, S. M. Wiltgen, I. Parker, Localization of puff sites adjacent to the plasma membrane: Functional and spatial characterization of Ca^{2+} signaling in SH-SY5Y cells utilizing membrane-permeant caged IP_3 . *Cell Calcium* **45**, 65–76 (2010).
- S. L. Dargan, I. Parker, Buffer kinetics shape the spatiotemporal patterns of IP_3 -evoked Ca^{2+} signals. *J. Physiol.* **553**, 775–788 (2003).
- K. L. Ellefsen, B. Settle, I. Parker, I. F. Smith, An algorithm for automated detection, localization and measurement of local calcium signals from camera-based imaging. *Cell Calcium* **56**, 147–156 (2014).
- I. Parker, Y. Yao, V. Ilyin, Fast kinetics of calcium liberation induced in *Xenopus* oocytes by photoreleased inositol trisphosphate. *Biophys. J.* **70**, 222–237 (1996).
- S. Bergmann, O. Sandler, H. Sberro, S. Shneider, E. Schejter, B.-Z. Shilo, N. Barkai, Pre-steady-state decoding of the Bicoid morphogen gradient. *PLOS Biol.* **5**, e46 (2007).
- E. Decrock, M. De Bock, N. Wang, A. K. Gadicherla, M. Bol, T. Delvaeye, P. Vandenabeele, M. Vinken, G. Bultynck, D. V. Krysko, L. Leybaert, IP_3 , a small molecule with a powerful message. *Biochim. Biophys. Acta* **1833**, 1772–1786 (2013).
- L. Gelens, G. A. Anderson, J. E. Ferrell, Spatial trigger waves: Positive feedback gets you a long way. *Mol. Biol. Cell* **25**, 3486–3493 (2014).
- V. Konieczny, M. V. Keebler, C. W. Taylor, Spatial organization of intracellular Ca^{2+} signals. *Semin. Cell Dev. Biol.* **23**, 172–180 (2012).
- M. Kruse, O. Vivas, A. Traynor-Kaplan, B. Hille, Dynamics of phosphoinositide-dependent signaling in sympathetic neurons. *J. Neurosci.* **36**, 1386–1400 (2016).
- S. S. Wang, A. A. Alousi, S. H. Thompson, The lifetime of inositol 1,4,5-trisphosphate in single cells. *J. Gen. Physiol.* **105**, 149–171 (1995).
- J. K. Foskett, C. White, K.-H. Cheung, D.-O. D. Mak, Inositol trisphosphate receptor Ca^{2+} release channels. *Physiol. Rev.* **87**, 593–658 (2007).
- S. P. Dawson, J. Keizer, J. E. Pearson, Fire-diffuse-fire model of dynamics of intracellular calcium waves. *Proc. Natl. Acad. Sci. U.S.A.* **96**, 6060–6063 (1999).
- L. Leybaert, M. J. Sanderson, Intercellular Ca^{2+} waves: Mechanisms and function. *Physiol. Rev.* **92**, 1359–1392 (2012).
- J. T. Lock, I. Parker, I. F. Smith, Communication of Ca^{2+} signals via tunneling membrane nanotubes is mediated by transmission of inositol trisphosphate through gap junctions. *Cell Calcium* **60**, 266–272 (2016).
- S. Manita, W. N. Ross, IP_3 mobilization and diffusion determine the timing window of Ca^{2+} release by synaptic stimulation and a spike in rat CA1 pyramidal cells. *Hippocampus* **20**, 524–539 (2010).
- W. N. Ross, Understanding calcium waves and sparks in central neurons. *Nat. Rev. Neurosci.* **13**, 157–168 (2012).
- K. J. Reissner, L. Pu, J. H. Schaffhausen, H. D. Boyle, I. F. Smith, I. Parker, T. J. Carew, A novel postsynaptic mechanism for heterosynaptic sharing of short-term plasticity. *J. Neurosci.* **30**, 8797–8806 (2010).
- M. J. Hubley, R. C. Rosanske, T. S. Moerland, Diffusion-coefficients of ATP and creatine-phosphate in isolated muscle: Pulsed gradient ^{31}P NMR of small biological samples. *NMR Biomed.* **8**, 72–78 (1995).
- E. A. Finch, G. J. Augustine, Local calcium signalling by inositol-1,4,5-trisphosphate in Purkinje cell dendrites. *Nature* **396**, 753–756 (1998).

31. N. Callamaras, I. Parker, Inositol 1,4,5-trisphosphate receptors in *Xenopus laevis* oocytes: Localization and modulation by Ca^{2+} . *Cell Calcium* **15**, 66–78 (1994).
32. S. Kume, A. Muto, J. Aruga, T. Nakagawa, T. Michikawa, T. Furuichi, S. Nakade, H. Okano, K. Mikoshiba, The *Xenopus* IP_3 receptor: Structure, function, and localization in oocytes and eggs. *Cell* **73**, 555–570 (1993).
33. J. Crank, *The Mathematics of Diffusion* (Oxford Univ. Press, ed. 2, 1979).
34. Z. Ding, A. M. Rossi, A. M. Riley, T. Rahman, B. V. L. Potter, C. W. Taylor, Binding of inositol 1, 4, 5-trisphosphate (IP_3) and adenophostin A to the N-terminal region of the IP_3 receptor: Thermodynamic analysis using fluorescence polarization with a novel IP_3 receptor ligand. *Mol. Pharmacol.* **77**, 995–1004 (2010).
35. I. Parker, I. F. Smith, Recording single-channel activity of inositol trisphosphate receptors in intact cells with a microscope, not a patch clamp. *J. Gen. Physiol.* **136**, 119–127 (2010).
36. K. J. Alzayady, L. Wang, R. Chandrasekhar, L. E. W. li, F. Van Petegem, D. I. Yule, Defining the stoichiometry of inositol 1,4,5-trisphosphate binding required to initiate Ca^{2+} release. *Sci. Signal.* **9**, ra35 (2016).
37. J. Keener, J. Sneyd, *Mathematical Physiology* (Springer, 2009).

Acknowledgments: We thank N. Hengartner and D. Colquhoun for helpful discussions and B. Settle for help with software development. **Funding:** This work was supported by

the NIH through grants R37 GM048071 (to I.P.), RO1 GM065830 (to J.E.P. and I.P.), and F31 GM119330-01 (to K.E.); and by UBA and FONCyT (Argentina) through grants UBACyT 20020130100480BA and PICT 2013-1301 (to S.D.). **Author contributions:** G.D.D. performed experiments and analyzed experimental data. K.L.E. wrote analytical and simulation software and together with G.D.D. performed numerical simulations. J.E.P. and S.P.D. formulated the analytical solutions and performed statistical analysis. I.P. conceived and supervised the project. All authors contributed to writing the paper and read and approved the final manuscript. **Competing interests:** The authors declare that they have no competing interests. **Data and software availability:** Raw data and custom software are freely available to academic researchers upon request.

Submitted 31 May 2016

Accepted 19 October 2016

Published 8 November 2016

10.1126/scisignal.aag1625

Citation: G. D. Dickinson, K. L. Ellefsen, S. P. Dawson, J. E. Pearson, I. Parker, Hindered cytoplasmic diffusion of inositol trisphosphate restricts its cellular range of action. *Sci. Signal.* **9**, ra108 (2016).

Hindered cytoplasmic diffusion of inositol trisphosphate restricts its cellular range of action

George D. Dickinson, Kyle L. Ellefsen, Silvina Ponce Dawson, John E. Pearson and Ian Parker (November 8, 2016)
Science Signaling **9** (453), ra108. [doi: 10.1126/scisignal.aag1625]

The following resources related to this article are available online at <http://stke.sciencemag.org>.
This information is current as of November 12, 2016.

- Article Tools** Visit the online version of this article to access the personalization and article tools:
<http://stke.sciencemag.org/content/9/453/ra108>
- Supplemental Materials** "*Supplementary Materials*"
<http://stke.sciencemag.org/content/suppl/2016/11/04/9.453.ra108.DC1>
- Related Content** The editors suggest related resources on *Science's* sites:
<http://stke.sciencemag.org/content/sigtrans/9/453/fs17.full>
<http://stke.sciencemag.org/content/sigtrans/9/422/ra35.full>
- References** This article cites 35 articles, 17 of which you can access for free at:
<http://stke.sciencemag.org/content/9/453/ra108#BIBL>
- Permissions** Obtain information about reproducing this article:
<http://www.sciencemag.org/about/permissions.dtl>